Available online at www.ilcpa.pl

International Letters of Chemistry, Physics and Astronomy

13 (2013) 90-102 ISSN 2299-3843

Structural, Morphological and Optical Characterization of SnO_2:F thin films prepared by Chemical spray Pyrolysis

Salam Amir Yousif, Jenan Mohamed Abass

Department of Physics, College of Education, Al-Mustansiriyah University, Baghdad, Iraq

E-mail address: Salamamir90@yahoo.com

ABSTRACT

Fluorine doped tin oxide (FTO) films were successfully prepared on glass and quartz substrate at a substrate temperature equal to 450 ℃ for different fluorine doping (0, 0.05, 0.1, 0.15) by a homemade spray pyrolysis technique. The spray solution prepared from tin tetrachloride pentahydrate ($SnCl_4 \cdot 5H_2O$) dissolved in distilled water at ($0.1\ M$) concentration and ammonium fluoride (NH_4F) was added into the solution for fluorine doping. X-ray diffraction patterns of the spray-deposited (SnO_2: F) films for different fluorine doping show that all the diffractograms contain the characteristic SnO_2 orientations. The matching of the observed and standard d-values confirm that the deposited films are of tin oxide with tetragonal structure and the films are polycrystalline with (110) as a preferred growth orientation. The surface morphology of $SnO_2:F$ thin film has been examined by atomic force microscopy (AFM). The average transmittance in the visible region (at 550 nm) has been found (40 %, 47 %, 52 %, 59 %, 61 %) for the fluorine doping (0, 0.05, 0.1, 0.15, 0.2) respectively.

***Keywords*:** SnO_2; SnO_2:F; X-ray Diffraction; Optical Characterization

1. INTRODUCTION

Transparent conducting oxide (TCO) thin films such as zinc oxide, indium oxide, tin oxide, indium tin oxide and cadmium oxide have attracted considerable attention because of their low resistivity and high transmittance [1]. Due to their optical and electrical properties, TCOs are used for photovoltaic solar cells, phototransistors, liquid crystal displays, optical heaters, gas sensors, transparent electrodes and other optoelectronic devices [2-9]. Among these TCOs SnO_2 films are inexpensive, chemically stable in acidic and basic solutions, thermally stable in oxidizing environments at high temperatures and also mechanically strong, which are important attributes for the fabrication and operation of solar cells [10-12]. SnO_2 has a tetragonal structure, similar to the rutile structure with the wide energy gap of $E_g = 3.6 - 4\ eV$ and behaves as an n-type semiconductor [13-15]. Antimony (Sb), arsenic (As), phosphorus (P), indium (In), molybdenum (Mo), fluorine (F), and chlorine (Cl) have been selected as doping elements for SnO_2 films [16-23]. SnO_2 thin films are produced by different techniques such as thermal evaporation, sputtering, spray pyrolysis, sol-gel and hydrothermal

[24-33]. Among these, spray pyrolysis is well suited for the preparation of doped tin oxide thin films because of its simple and inexpensive experimental arrangement, ease of adding various doping materials, reproducibility, high growth rate and mass production capability for uniform large area coatings [1,34].

2. EXPERIMENTAL PART

Fluorine doped tin oxide (FTO) films were prepared on glass and quartz substrate ($2.5 \times 2.5\ cm^2$) at a substrate temperature (450 ℃) for different fluorine doped (0, 0.05, 0.1, 0.15) by a homemade spray pyrolysis technique under ambient atmosphere. The experimental setup and other details have been reported elsewhere [35]. The spray solution prepared from tin tetrachloride penthydrate ($SnCl_4 \cdot 5H_2O$) dissolved in distilled water at ($0.1\ M$) concentration and ammonium fluoride (NH_4F) was added into the solution for fluorine doping. The deposition parameters were the same for the series of $SnO_2{:}F$ films. The crystal structure and crystallinity of as-grown (FTO) films were investigated by X-ray diffraction (XRD) using SHIMADZU X-Ray diffractometer system (XRD - 6000), which record the intensity as a function of Bragg's angle. The surface morphology of ($SnO_2{:}F$) thin film has been examined by using atomic force microscopy (AFM, scanning probe microscope). The optical measurements of the SnO_2: F thin film are calculated from the transmittance and absorbance spectrum at normal incidence over the range (300 – 900 nm), by using UV-VIS spectrophotometer type (SHIMADZU) (UV-1600/1700 series).

3. RESULTS AND DISCUSSION

3. 1. Structural characterization

3. 1. 1. X-ray Diffraction (XRD)

Since changes in the structural properties of SnO_2 films can be correlated with the variations of the electrical and optical properties, x-ray diffraction measurements were made to determine the d-values, crystallographic structure, lattice parameters, grain size, texture coefficient and others. XRD patterns obtained for the films grown on glass substrate at a substrate temperature equal to (450 ℃) were studied in the (2θ) range of ($20 – 70°$). Figure (1) depicts the x-ray diffraction patterns of spray-deposited $SnO_2{:}F$ thin films for different fluorine doping. All the diffractograms contain the characteristic SnO_2 orientations. The observed d-values are presented in table (1) and compare with the standard ones from the (JCPDS) data files [36]. The matching of the observed and standard d-values confirms that the deposited films are of tin oxide with tetragonal structure.

The x-ray diffraction spectra of (SnO_2: F) films for different fluorine doping levels in the precursor solution shows that the films are polycrystalline with (110) as a preferred growth orientation. The (110) peak is the strongest peak observed in all the films, the presence of other peaks such as (101), (200) and (211) have also been detected but with substantially lower intensities. The presence of other phases such as (SnO, Sn and SnF_2) is not detected, indicating the (O) atoms were replaced by (F) atoms in the (SnO_2: F) films [37,38,42-46]. The introduction of fluorine does not affect the structural properties of the films, however, the decrease in the intensities of the main XRD peaks with increasing fluorine doping levels, is probably attributed to the change in the growth rate which leads to a decrease in the thickness of the $SnO_2{:}F$ films.

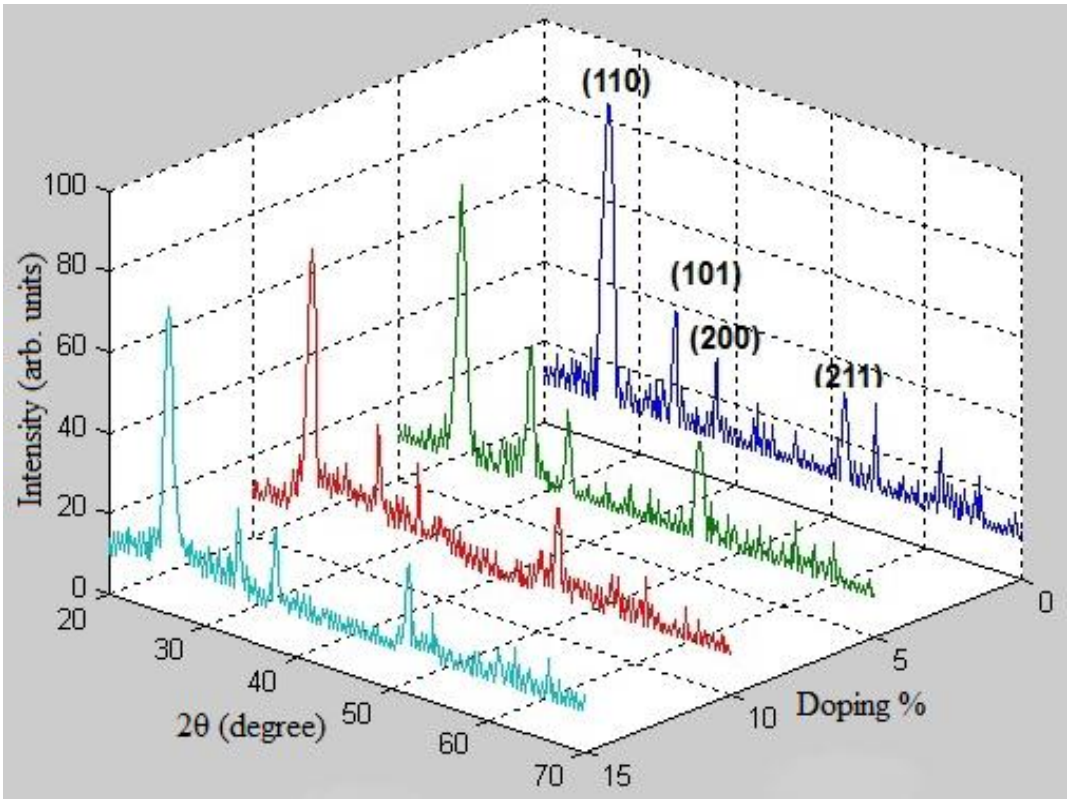

Fig. 1. X-ray diffraction patterns of (SnO_2: F) thin films for different fluorine doping.

Table 1. XRD parameters of ASTM and prepared ($SnO_2:F$) thin films deposited on glass substrate at 450 ℃.

Doping			0 %	5 %	10 %	15 %	ASTM (SnO_2)
(hkl)	(110)	2θ (deg.)	26.5449	26.5683	26.5666	26.5383	26.611
		d (Å)	3.35523	3.35233	3.35254	3.35605	3.35
		Int.	100	100	100	100	100
	(101)	2θ (deg.)	33.7291	34.0788	33.7990	33.8390	33.893
		d (Å)	2.65520	2.62875	2.64987	2.64683	2.644
		Int.	22	32	28	28	75
	(200)	2θ (deg.)	37.8255	38.0603	37.8555	37.8155	37.949
		d (Å)	2.37653	2.36241	2.37472	2.37714	2.369
		Int.	19	23	17	17	21
	(211)	2θ (deg.)	51.8074	51.7674	51.8074	51.7375	51.780
		d (Å)	1.76327	1.76453	1.77058	1.76548	1.765
		Int.	25	32	28	28	57

3. 1. 2 Lattice Parameters

The lattice constant (a) and (c) of the $SnO_2:F$ thin films for different fluorine doping determined from equation (1) and the ratio of (c/a) belong to the (110) plane as a preferred orientation have been listed in Table (2), found to be in a good agreement with the reported and the standard (JCPDS) values. It is also found that the lattice constant (a) increase slightly with increasing fluorine doping in the films, while there are an arbitrary changed in the lattice constant (c) with increasing fluorine doping. Figures [2, 3] show the lattice constant (a) and (c) as a function of fluorine content in the films.

$$\frac{1}{d^2} = \frac{h^2+k^2}{a^2} + \frac{l^2}{c^2} \quad \ldots\ldots (1)$$

Table 2. Lattice constants of (SnO_2: F) thin films deposited for different fluorine doping at a substrate temperature (450 ℃).

Samples	Fluorine Doping (%)	a (Å)	c (Å)	(c/a)
1	0	4.74003	3.1959241	0.6742408
2	5	4.74091055	3.1588125	0.666288135
3	10	4.74120754	3.1955645	0.673998024
4	15	4.74617143	3.1887284	0.671852775
(JCPDS)	**0**	4.73761543	3.1863765	0.672569684

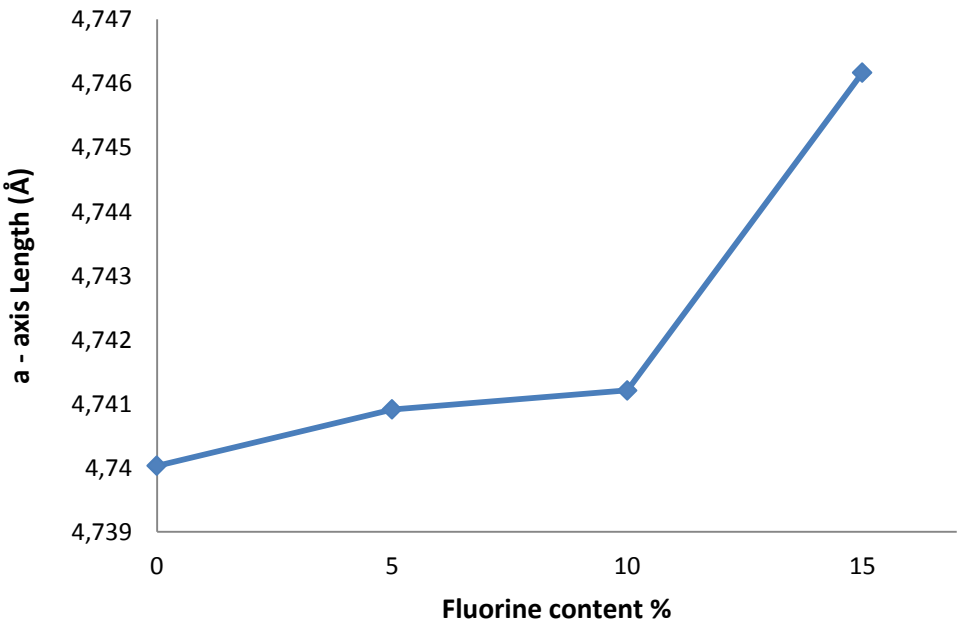

Fig. 2. a-axis length vs. fluorine content.

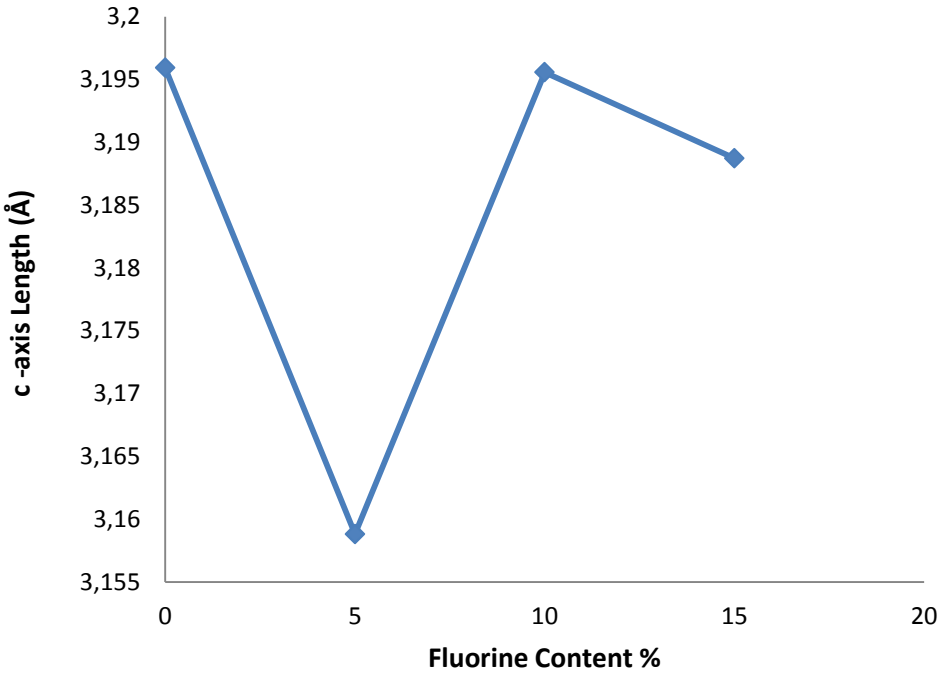

Fig. 3. c-axis length vs. fluorine content.

3. 1. 3. Grain Size (D)

The crystallite size is estimated by using Scherrer's formula given by equation (2) [38].

$$D = \frac{k\lambda}{\beta cos\theta} \quad \text{..... (2)}$$

where k varies from 0.89 to 1.39. But in most of the cases it is closer to 1. Hence for grain size calculation it is taken to be 0.94, λ is the wavelength of x-ray, β is the full width at half of the peak maximum in radian and θ is Bragg's angle (in degree).

It is observed that crystalline size increases initially with an increase in fluorine doping in the films reaches the maximum (5.29) nm at (0.10) fluorine doping and thereafter it goes on decreasing with increases in fluorine content in the films.

The values of crystallite size for different fluorine content are shown in Table 3 and depicted in Figure 4.

3. 1. 4 Full Width at Half Maximum (FWHM)

The full width at half maximum of the preferred orientation (peak) could be measured, since it is equal to the width of the line profile (in degrees) at the half of the maximum intensity.

The values of FWHM of the preferred orientation (110) have been measured and listed in Table 3.

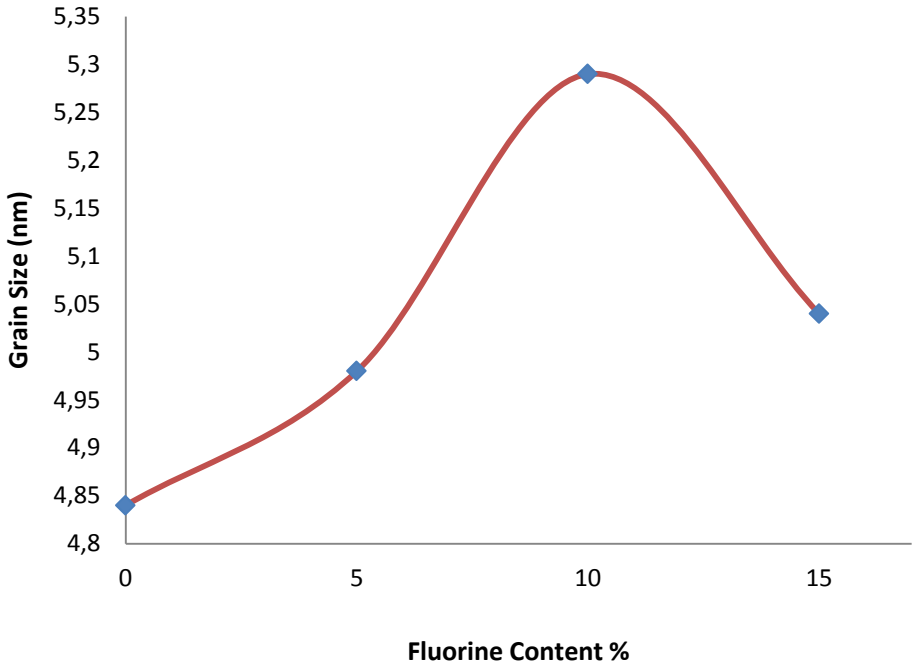

Fig. 4. Grain size vs. fluorine content.

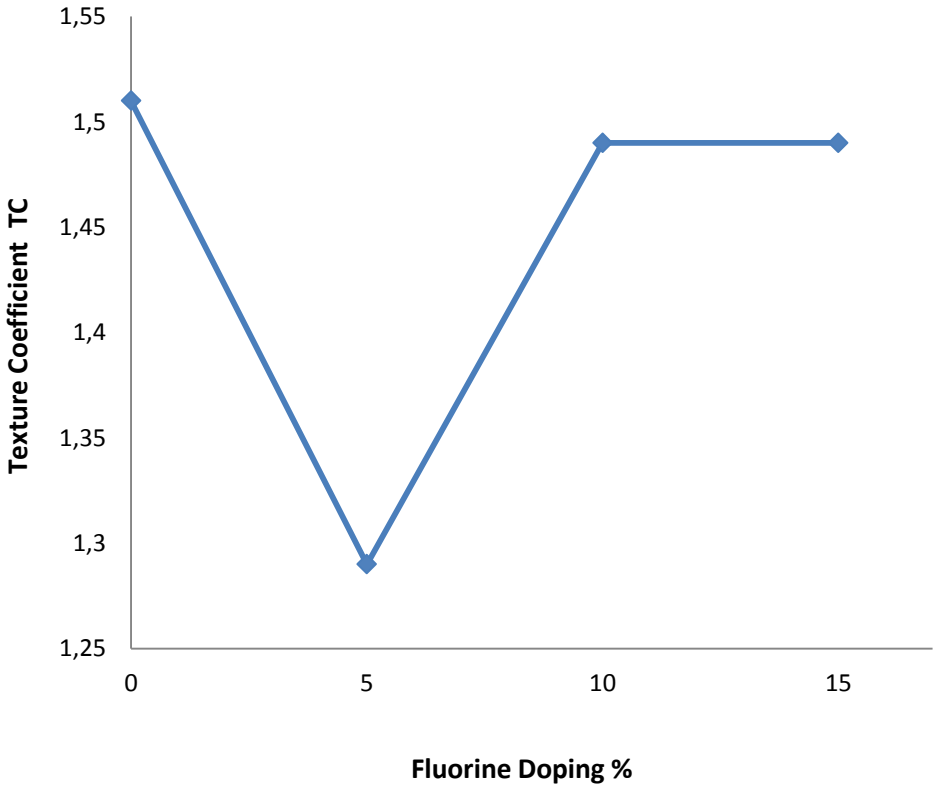

Fig. 5. Texture coefficient vs. fluorine doping.

3. 1. 5 Texture Coefficient (TC)

The texture coefficient defined by Barret and Massalski [39] has been used to describe the preferred orientation.

$$TC(hkl) = \frac{I(hkl)/I_0(hkl)}{N_r^{-1}\sum_N I(hkl)/I_0(hkl)} \quad \ldots\ldots\ldots (3)$$

where TC is the texture coefficients of the (*hkl*) plane, $I_{(hkl)}$ the measured intensity, $I_{0(hkl)}$ the ASTM standard intensity of the corresponding powder, and N is the reflection number of significant peaks. From this definition it is clear that the deviation of the texture coefficient from the unity implies the preferred orientation of the growth. The larger of texture coefficient deviates from unity, the higher will be the preferred orientation of a film. The variation of texture coefficient estimated along (110) direction with the fluorine content for SnO_2: F thin films are shown in Figure 5 and listed in Table 3. It is seen that the texture coefficient decrease with adding fluorine atoms in the SnO_2 films and it will increase with the increasing in fluorine doping in the films reaches to a constant value for the (10 %, 15 %) fluorine-doping films.

3. 1. 6 Micro strain (ε)

The micro strain is caused during the growth of thin films, and will be raised from stretching or compression in the lattice to make a deviation in the c-lattice constant of the tetragonal structure from ASTM value. So the strain broadening is caused by varying the displacement of atoms with respect to their reference lattice position. This strain can be calculated from then following equation [40]. The values of micro strain of the SnO_2: F films have been calculated and listed in Table (3).

$$\langle \varepsilon \rangle = \frac{\left| C_{ASTM} - C_{XRD} \right|}{C_{ASTM}} \times 100\% \quad \ldots\ldots\ldots\ldots (4)$$

3. 1. 7. Integral Breadth (B)

The integral breadth of the samples has been obtained from XRD pattern. The values of integral breadth are recorded in table (3) and are calculated by using the following equation [41].

$$\mathbf{B} = \frac{\boldsymbol{Area}}{\boldsymbol{I_o}} \quad \ldots\ldots\ldots\ldots (5)$$

where: Area = area under peak, I_o = maximum intensity

3. 1. 8 Shape Factor (Φ)

The shape factor of the line profile resulting from the x-ray diffraction patterns could be calculated from the following relation [41] and are listed in table (3).

$$\Phi = \frac{FWHM}{Integral\ Breadth} \quad \ldots\ldots\ldots\ldots (6)$$

Table 3. Structural properties of SnO_2: F thin films deposited at (450 ℃).

Sample	*Doping %*	*Grain Size (D) (nm)*	*Micro Strain (ε) %*	*TC (110)*	*FWHM (degree)*	*Integral Breadth*	*Shape Factor (Φ)*
1	0	4.84	0.279	1.517	1.6867	1.64	1.028
2	5	4.98	0.909	1.297	1.64	1.68	0.976
3	10	5.29	0.268	1.495	1.5433	1.34	1.151
4	15	5.04	0.053	1.495	1.62	1.33	1.218

3. 2. Film Morphology

The surface morphology of $SnO_2:F$ thin films for different fluorine-doping (0, 0.05, 0.1, 0.15) deposited on ga glass substrateat a substrate temperature (450 ℃) has been examined by atomic force microscopy (AFM, scanning probe microscope). The three-dimensional (3D) topographic views of AFM images for $SnO_2:F$ films are shown in figure (6).

The films reveal homogenous surface and the grains were elongated from the inner towards the surface and, the root mean square (RMS) roughness for $SnO_2:F$ are (1.09, 1.07, 0.94, 0.69) nm for the fluorine doping (0, 0.05, 0.1, 0.15) respectively. The AFM study showed that the RMS roughness of undoped films reduced considerably from 1.09 to 0.69 nm due to fluorine doping (0.15), and the results showed that the values of the RMS roughness of the present work are smaller than the results obtained from another report [1], which makes a suitable reason to use it in solar cell applications.

The grain size of (SnO_2: F) thin films were evaluated at (78, 92, 97, 95) nm for fluorine-doping (0, 0.05, 0.1, 0.15) respectively. Grain size was less than (100 nm) which confirms the presence of nanostructures. AFM study reveals that the roughness of the film is dependent on the concentration of the dopant.

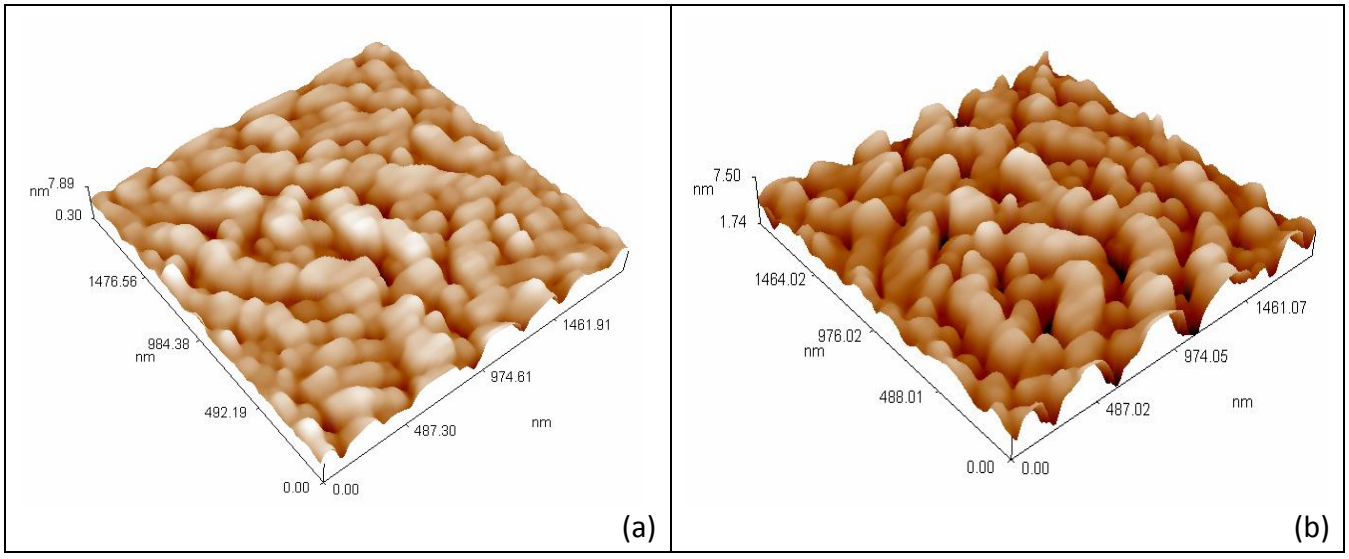

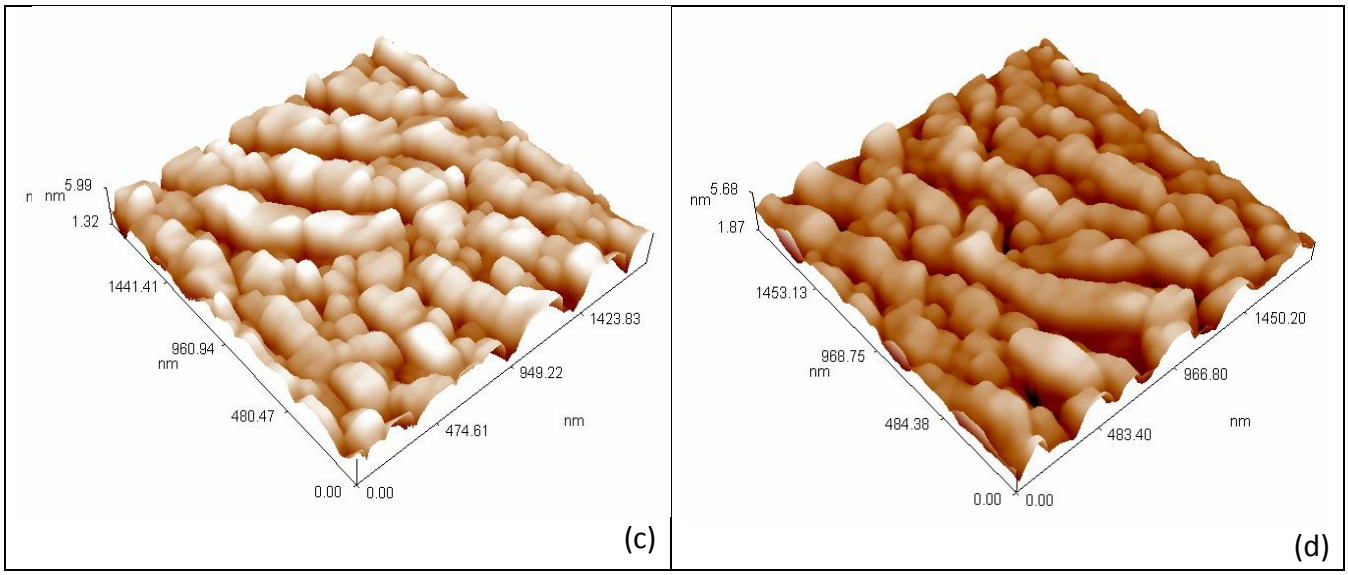

Fig. 6. The AFM images of $SnO_2:F$ thin film for different fluorine-doping (a) F = 0, (b) F = 0.05, (c) F = 0.1 and (d) F = 0.15

3. 3. Optical characterization

The optical properties of $SnO_2:F$ thin films prepared with different fluorine-doped (0, 0.05, 0.1, 0.15, 0.2) by spray pyrolysis technique on quartz substrate at substrate temperature (450 ℃) have been investigated by the room temperature transmission and absorption spectra were measured in the range from (300 nm to 900 nm).

3. 3. 1. Transmittance

The UV-visible transmittance spectra of $SnO_2:F$ thin films as a function of wavelength for different fluorine doping have been shown in Figure 7. It is seen that the transmittance of the $SnO_2:F$ films increases with increasing fluorine dopant in the films, and the average transmittance in the visible region (at 550 nm) has been found (40 %, 47 %, 52 %, 59 %, 61 %) for the fluorine doping (0, 0.05, 0.1, 0.15, 0.2) respectively. The transmittance value of 50 % for the undoped films found increased to 70 % for 0.20 of fluorine doping (at 890 nm). The increase in the transmittance spectra of the $SnO_2:F$ due to the decreasing in the film thickness because of the growth rate is decreased with increase fluorine content in the films and, the color of the undoped tin oxide thin film is milky white that turned colorless When the doping concentration increased to (20 %), which is in a good agreement with the report [1].

3. 3. 2. Optical Bandgap (E_g)

The optical bandgap (E_g) of the $SnO_2:F$ thin films was calculated from the allowed direct transition given by [1].

$$\alpha h\gamma = A(h\gamma - E_g)^{1/2} \quad \ldots\ldots\ldots (7)$$

where α (cm^{-1}) is the absorption coefficient, h (J.s) is Planck's constant, γ (Hz) is the photon frequency, A is the edge parameter, and E_g (eV) is the bandgap energy.

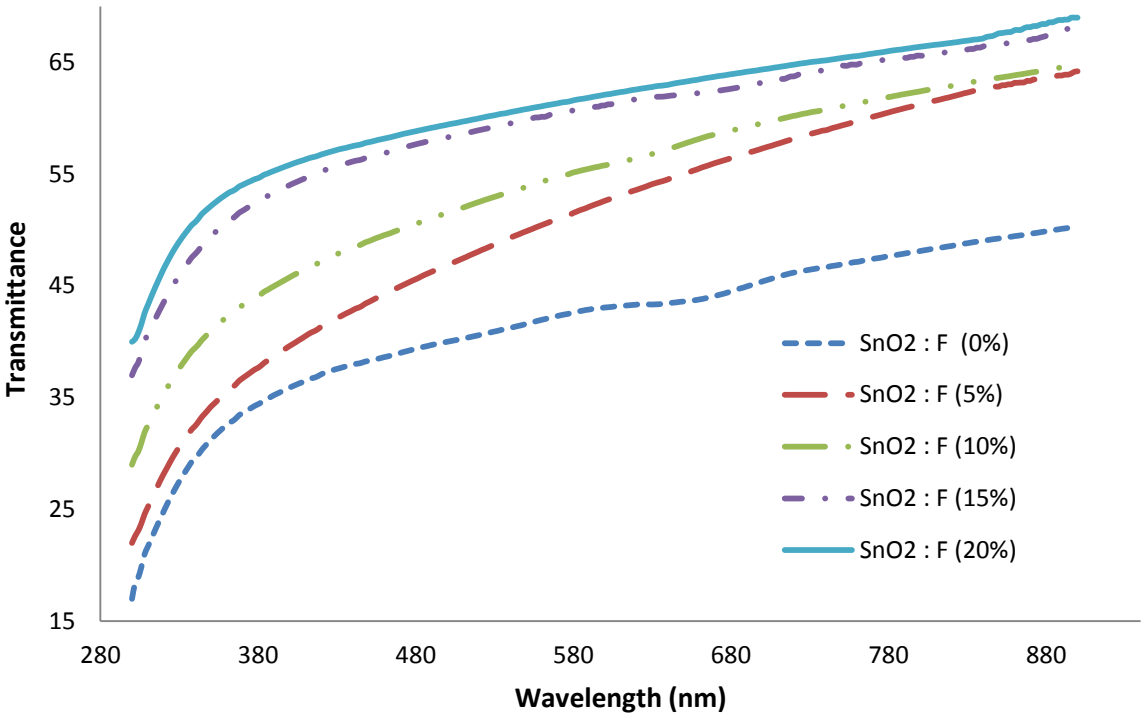

Fig. 7. Transmittance spectra of $SnO_2:F$ thin films as a function of wavelength for different fluorine doping.

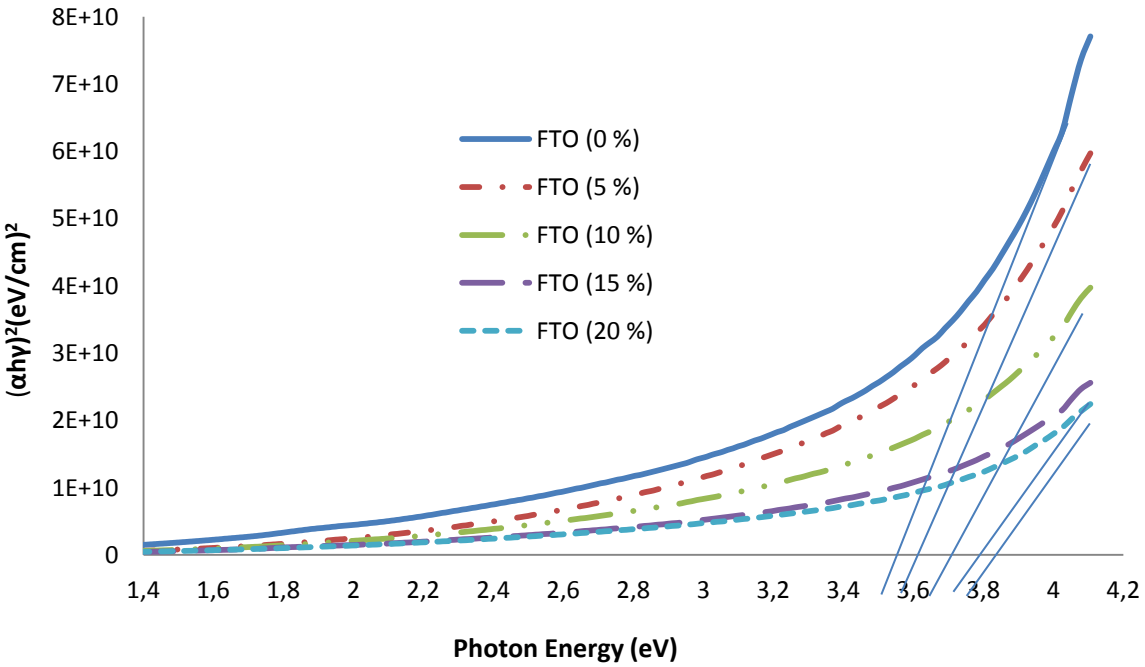

Fig. 8. Optical bandgap of SnO_2: F thin films as a function of photon energy for different fluorine doping.

The optical bandgap is determined by extrapolating the linear part of the curve $(\alpha h\gamma)^2$ which intercepts the energy axis, E_g are found to be (3.5, 3.57, 3.65, 3.7, 3.75) eV for the (0,5 %, 10 %, 15 %, 20 %) fluorine doping concentration respectively as shown in Figure 8. As can be clearly seen in Figure 8 the optical bandgap is increasing with the increase in fluorine doping concentration in the films. This result is in a good agreement with the report results obtained by Elangovan and Ramamurthi [1].

4. CONCLUSIONS

Fluorine doped tin oxide (FTO) films were successfully prepared on glass and quartz substrate at a substrate temperature equal to 450 ℃ by a homemade spray pyrolysis technique. All the diffractograms contain the characteristic SnO_2 orientations. The x-ray diffraction spectra of (SnO_2: F) films for different fluorine doping levels in the precursor solution shows that the films are polycrystalline with (110) as a preferred growth orientation. The introduction of fluorine does not affect the structural properties of the films, however, the decrease in the intensities of the main XRD peaks with increasing fluorine doping levels, is probably attributed to the change in the growth rate which leads to a decrease in the thickness of the $SnO_2{:}F$ films. The AFM study showed that the RMS roughness of undoped films reduced considerably from 1.09 to 0.69 nm due to fluorine doping (0.15). The transmittance value of 50 % for the undoped films found increased to 70 % for 0.20 fluorine doping (at 890 nm). The increase in the transmittance spectra of the $SnO_2{:}F$ due to the decreasing in the film thickness because of the growth rate is decreased with increase fluorine content in the films.

References

[1] E. Elangovan, K. Ramamurthi, Appl. Surf. Sci. 249 (2005) 183.

[2] F. Atay, M. Demir, S. Kose, V. Bilgin, I. Akyuz, *J. Optoelectron. Adv. M.* 9(7) (2007) 2217.

[3] J. Isidorsson, C.G. Granqvist, *Sol. Energy. Mat. Sol.* C 44 (1996) 375.

[4] K.L. Chopra, S. Major, D.K. Pandya, *Thin Solid Films* 102 (1983) 1.

[5] C.G. Granqvist, *Handbook of Inorganic Electronic Materials,* Elsevier Puplication, The Netherlands, 1995.

[6] B. Stjerna, E. Olsson, C.G. Granqvist, *J. Appl. Phys.* 76 (1994) 3797.

[7] V. Vasu, A. Subrahmanyam, *Thin Solid Films* 193-194 (1990) 973.

[8] C. Li, B. Hua, *Thin Solid Films* 310 (1997) 238.

[9] B. Thangaraju, *Thin Solid Films* 402 (2002) 71.

[10] H. Kim, R.C.Y. Auyeung, A. Pique, *Thin Solid Films* 516 (2008) 5052.

[11] Arturo I. Martinez, Dwight R. Acosta, *Thin Solid Films* 483 (2005) 107.

[12] Houng-Lei Ma, Xiao-Tao Hao, J. Ma, Ying-Ge Yang, J. Huang, De-Heng Zhang, Xian-Gang Xu, *Appl. Surf. Sci.* 191 (2002) 313.

[13] A.V. Moholkar, S.M. Pawar, K.Y. Rajpure, C.H. Bhosale, *Mater. Lett.* 61 (2007) 3030.

[14] Sung-Sik Chang, M.S. Jo, *Ceram. Int.* 33 (2007) 511.

[15] Z.B. Zhou, R.Q. Cui, Q.J. Pang, Y.D. Wang, F.Y. Meng, T.T. Suna, Z.M. Dingb, X.B. Yu, *Appl. Surf. Sci.* 172 (2001) 245.

[16] H. Kim, A. Pique, *Appl. Phys. Lett.* 84 (2004) 218.

[17] S. R. Vishwakarma, J.P. Upadhyay, H.C. Prasad, *Thin Solid Films* 176 (1989) 99.

[18] J.P. Upadhyay, S.R. Vishwakarma, H.C. Prasad, *Thin Solid Films* 167 (1988) 7.

[19] P.K. Manoj, B. Joseph, V.K. Vaidyan, D.S.D. *Amma, Ceram. Int.* 33 (2007) 273.

[20] S. Suporthina, M.R. De Guire, *Thin Solid Films* 371 (2000) 1.

[21] H.L. Hartnagel, A.L. Dawar, A.K. Jain, C. Jagadish, *Semiconducting Transparent Thin Films,* Institute of Physics Publishing, Bristol, (1995).

[22] Te-Hua Fang, Win-Jin Chang, *Appl. Surf. Sci.* 220 (2003) 175.

[23] B.J. Lokhande, D. Uplane, *Appl. Surf. Sci.* 167 (200) 243.

[24] D.R. Acosta, E.P. Zironi, E. Montoya, W. Estrada, *Thin Solid Films* 288 (1996) 1.

[25] T. Schuler, M.A. Aegerter, *Thin Solid Films* 351 (1999) 125.

[26] K. Kim,T.G. Finstad, W.K. Chu, X.B. Cox, R,W. Linton, *Solar Cells* 13 (1984) 301.

[27] S. Ghosh, H. Kim, K. Hang, C. Lee, Mater Sci. Eng., B, *Solid-State Mater. Adv. Technol.* 95 (2002) 171.

[28] M. Okuya, *J. Eur. Ceram. Soc.* 21 (2001) 2099.

[29] J.R. Brown, P.W. Haycock, L.M. Smith, A.C. Jones, E.W. Williams, *Sens. Actuators B, Chem*. 63 (2000) 109.

[30] O.K. Varghese, L.K. Malhotra, *J. Appl. Phys.* 87 (2000) 7457.

[31] Q. Chen, Y. Qian, Z. Chen, G. Zhou, Y. Zhang, *Thin Solid Films* 264 (1995) 25.

[32] M. Kojima, H. Kato, M. Gatto, *Pilos. Mag. B* 68 (1993) 215.

[33] H. Cachet, J. Bruneaux, G. Folcher, C. Levy-Clement, C. Vard, M. Neumann-Spallart, *Sol. Energ. Mat. Sol.* C. 46 (1997) 101.

[34] I. Taniguchi, D. Song, M. Wakihara, *J. Power Sources* 109 (2002) 333.

[35] P.S. Patil, *Mater. Chem. Phys.* 59 (1999) 185.

[36] Powder Diffraction File Alphabetic PDF-2 Data Base,file41-1445, International center of Diffraction Data, Newtown Square, PA, USA, 1994.

[37] D.W. Sheel, H.M. Yates, P. Evans, U. Dagkaldiran, A. Gordijn, F. Finger, Z. Remes, M. Vanecek, *Thin Solid Films* 517 (2009) 3061-3065.

[38] A.A. Yadav, E.U. Masumdar, A.V. Moholkar, M. Neumann-Spallart, K.Y. Rajpure, C.H. Bhosale, *J. Alloys Compd.* 488 (2009) 350-355.

[39] C. Barret, T.B. Massalski, Structure of Metals, Pergamon, Oxford, 1980, (923p).

[40] T. Obata, K. Komeda, T. Nakao, H. Ueba, and C. Tasygama, *J. Appl. Phys.* 81 (1997) 199.

[41] P. Šutta, Q. Jackuliak, *Mater. Struct.* 5(1) (1998) 10-14.

[42] Saad F. Oboudi, Nadir F. Habubi, Ghuson H. Mohamed, Sami S. Chiad, *International Letters of Chemistry, Physics and Astronomy* 8(1) (2013) 78-86.

[43] Sujan Kumar Das, Jahid M. M. Islam, Monirul Hasan, Humayun Kabir, Md. Abdul Gafur, Enamul Hoque, Mubarak A. Khan, *International Letters of Chemistry, Physics and Astronomy* 10(1) (2013) 90-101.

[44] J. A. Najim, J. M. Rozaiq, *International Letters of Chemistry, Physics and Astronomy* 10(2) (2013) 137-150.

[45] Majid H. Hassouni, Khudheir A. Mishjil, Sami S. Chiad, Nadir F. Habubi, *International Letters of Chemistry, Physics and Astronomy* 11 (2013) 26-37.

[46] C. Indira Priyadharsini, A. Prakasam, P. M. Anbarasan, *International Letters of Chemistry, Physics and Astronomy* 12 (2013) 82-93

(Received 27 August 2013; accepted 31 August 2013)